Seasonal and interannual variability of solar radiation at Spirit, Opportunity and Curiosity landing sites

Álvaro VICENTE-RETORTILLO[1], Mark T. LEMMON[2], Germán M. MARTÍNEZ[3], Francisco VALERO[4], Luis VÁZQUEZ[5], Mª Luisa MARTÍN[6]

[1]Departamento de Física de la Tierra, Astronomía y Astrofísica II, Universidad Complutense de Madrid, Madrid, Spain, alvarodv@ucm.es. [2]Department of Atmospheric Sciences, Texas A&M University, College Station, TX, USA, lemmon@tamu.edu. [3]Department of Climate and Space Sciences and Engineering, University of Michigan, Ann Arbor, MI, USA, gemartin@umich.edu. [4]Departamento de Física de la Tierra, Astronomía y Astrofísica II, Universidad Complutense de Madrid, Madrid, Spain, valero@ucm.es. [5]Departamento de Matemática Aplicada, Universidad Complutense de Madrid, Madrid, Spain, lvazquez@fdi.ucm.es. [6]Departamento de Matemática Aplicada, Universidad de Valladolid, Segovia, Spain, mlmartin@eii.uva.es.

Received: 14/04/2016
Accepted: 22/09/2016

Abstract
In this article we characterize the radiative environment at the landing sites of NASA's Mars Exploration Rover (MER) and Mars Science Laboratory (MSL) missions. We use opacity values obtained at the surface from direct imaging of the Sun and our radiative transfer model COMIMART to analyze the seasonal and interannual variability of the daily irradiation at the MER and MSL landing sites. In addition, we analyze the behavior of the direct and diffuse components of the solar radiation at these landing sites.
Key words: Solar radiation; Mars Exploration Rovers; Mars Science Laboratory; opacity, dust; radiative transfer model; Mars exploration.

Variabilidad estacional e interanual de la radiación solar en las coordenadas de aterrizaje de Spirit, Opportunity y Curiosity

Resumen
El presente artículo está dedicado a la caracterización del entorno radiativo en los lugares de aterrizaje de las misiones de la NASA de *Mars Exploration Rover* (MER) y de *Mars Science Laboratory* (MSL). Se hace uso de las opacidades obtenidas a partir de imágenes directas del Sol y de nuestro modelo de transferencia radiativa COMIMART con el fin de analizar la variabilidad estacional e interanual de la irradiación diaria en las coordenadas de aterrizaje de los MER y de MSL. Asimismo, se analiza el comportamiento de las componentes directa y difusa de la radiación solar en estos lugares de aterrizaje.
Palabras clave: Radiación solar; Mars Exploration Rovers; Mars Science Laboratory; opacidad; polvo; modelo de transferencia radiativa; exploración de Marte.

top of the atmosphere 4. Results: radiative environment at the MER and MSL landing sites 5. Conclusions. Acknowledgements. References.

Normalized reference
Vicente-Retortillo, A., Lemmon, M. T., Martínez, G. M., Valero, F., Vázquez, L., Martín, M. L. (2016). Seasonal and interannual variability of solar radiation at Spirit, Opportunity and Curiosity landing sites. *Física de la Tierra,* Vol., 28, 111-127.

Introduction

The study of the radiation environment at the Martian surface is important because of the role that solar radiation plays in constraining the habitability of Mars and in driving its atmospheric dynamics. Ultraviolet radiation has the potential to damage the DNA (Córdoba-Jabonero et al.,, 2003) while solar radiation feeds atmospheric thermodynamic processes occurring in the first meters of the Martian atmosphere, the so-called planetary boundary layer.

In this article we study the variability of the daily irradiation at the surface (also called insolation and defined as the total amount of solar energy received during one sol) at the landing sites of MER Spirit (14.57ºS, 175.48ºE) and Opportunity (1.95°S, 354.47°E) and MSL Curiosity (4.59ºS, 137.44ºE) rovers on seasonal and interannual time scales. We also discuss the variability of the diffuse and direct components of the insolation at these three locations.

In section 1 we review several efforts to retrieve dust opacity both from satellites and ground measurements, and we show the opacities at the Spirit, Opportunity and Curiosity landing sites. In section 2 we describe our COmplutense and MIchigan MArs Radiative Transfer model (COMIMART) and perform sensitivity studies to validate the assumption of using atmospheric optical depths as dust opacities. In section 3 we analyze the behavior of the total radiation at the top of the atmosphere. In section 4 we characterize the radiative environment at the three selected landing sites. Finally, we highlight our main conclusions in section 5.

1. Dust opacity measurements on Mars

An accurate characterization of suspended dust is essential for studies of the Martian atmosphere. The spatial distribution and radiative properties of dust have a strong impact on calculations of heating rates and thus on the atmospheric thermal behavior (Madeleine et al., 2011) and dynamical processes (Read and Lewis, 2004). Dust controls the amount of radiation that reaches the surface, which is the principal term of the energy budget at the surface of Mars (Martínez et al., 2014). This energy budget determines the diurnal cycle of the temperature of the ground (Savijärvi and Kauhanen, 2008; Martínez et al., 2009), which in turn affects the thermodynamic activity in the planetary boundary layer (Martínez et al., 2011). As an example, dust devils are more frequent on Mars when the insolation is higher and therefore the

surface is warmer, being therefore more frequent on Summer than at other times of the year (Petrosyan et al., 2011).

A wide number of efforts have been done to characterize the spatial and temporal variability of dust in the last decades. Advances in the characterization of dust have been mainly achieved from orbiter observations, but also from ground measurements. We now describe some of the main efforts regarding this matter.

In the early 70s, measurements by the Infrared Interferometer Spectrometer (IRIS) onboard Mariner 9 enabled the observation of the dissipation of the global dust storm in 1971 (Hanel et al., 1972). Between 1976 and 1979, data acquired by the Viking IR Thermal Mapper (IRTM) allowed global dust opacity mapping for more than 1.3 Martian years (Martin and Richardson, 1993); the results showed that there were two planet-encircling dust storms within this temporal range, known as 1977a and 1977b.

In 1999, the Thermal Emission Spectrometer (TES) onboard the Mars Global Surveyor (MGS) mission began to monitor the atmospheric conditions. Using TES measurements, Smith (2004) studied the interannual variability of dust opacity between 1999 and 2003. He concluded that during the aphelion season (solar longitude L_s between 0º and 180º), dust opacity is low and presents low interannual variability; in contrast, during the perihelion season (solar longitude L_s between 180º and 360º) the atmosphere is dustier and presents higher interannual variability.

More recently, infrared images acquired by the Thermal Emission Imaging System (THEMIS) onboard the Mars Odyssey mission over more than 3.5 years (between 2002 and 2008) were used by Smith (2009) to retrieve dust opacities. He showed that the dust activity during Mars Year 28 was markedly higher than in the previous two Mars Years (MY).

In 2006, the Mars Climate Sounder (MCS) onboard the Mars Reconnaissance Orbiter allowed additional retrievals of dust opacity. The combination of TES, THEMIS and MCS measurements has allowed producing a dust climatology from MY 24 to MY 31, covering the temporal range between April 1999 and July 2013 (Montabone et al., 2015).

Ground-based observations of opacity, although scarcer than from orbit, are very important because the retrieval process incorporates fewer assumptions than from orbit and thus the uncertainty in the results is lower, providing “ground truth” and complementary information for the analysis of satellite measurements.

Colburn et al. (1989) analyzed approximately 1.3 Martian years of Sun images acquired in the second half of the 70s at the two Viking landing sites, obtaining numerous values of the atmospheric opacity which showed a number of seasonal peaks.

Ten years later, Smith and Lemmon (1999) obtained atmospheric opacity values using direct images of the Sun by the Imager for Mars Pathfinder (IMP) during the 83-sol Mars Pathfinder mission. They provided hourly opacities between 07:00 and 17:00 LTST at four wavelengths: 450, 670, 883 and 989 nm, with values similar to those at the Viking sites.

Up to date, the most complete dataset of atmospheric opacity values obtained from ground measurements has been provided by the Pancam camera onboard the two

MER rovers. Using direct solar images of Sun, opacity values spanning more than 2200 sols for Spirit and more than 4300 sols (more than six Mars Years) for Opportunity have been retrieved (Lemmon et al., 2015). This optical depth record has been used as "ground truth" results in many studies, such as Wolff et al. (2009), Wolff et al. (2010) or Montabone et al. (2015). More recently, images of the Sun by the Mastcam instrument onboard MSL Curiosity rover are providing new aerosol opacity values at the MSL landing site.

From top to bottom, we show in Figure 1 atmospheric opacity values at the Spirit, Opportunity and Curiosity landing sites. At the three landing sites on each year, the perihelion season is dustier than the aphelion season. This seasonal behavior is in agreement with that derived from TES measurements (Smith, 2004). In particular, the lowest annual opacity values occur at L_s = 120º - 140º, while the highest annual values occur at L_s = 220º - 240º at the three landing sites. Opacities higher than 4 observed at the Spirit and Opportunity landing sites between L_s = 265º and L_s = 295º of MY 28 correspond to a global dust storm.

2. COMIMART Radiative Transfer model: Description and sensitivity studies

COMIMART is a new Martian radiative transfer model that we developed in 2015 and that we presented in Vicente-Retortillo et al. (2015). Our model enables the characterization of the radiative environment in different spectral regions in the solar range under different scenarios. In particular, it enables the calculation of spectral irradiances at the surface as well as the diurnal evolution of surface fluxes and daily irradiations. It also allows calculating the direct and diffuse components of solar radiation at the surface. COMIMART includes updated spectral radiative properties of atmospheric dust, water ice clouds and gas molecules. The input parameters of our model include dust opacity at 880 nm, water ice clouds opacity, abundance of the atmospheric gases, surface albedo, values at each wavelength of the radiative parameters (extinction efficiency, single scattering albedo and asymmetry factor), time of the day and of the year, latitude and spectral range.

The dust radiative parameters can be computed for any particle size distribution using Mie theory from spectral refractive indices. We have selected the refractive indices calculated by Wolff et al. (2009) and Wolff et al. (2010). The model assumes a log-normal particle size distribution, which is characterized by the effective radius and the dimensionless effective variance (Hansen and Travis, 1974). We have selected the canonical values for these parameters: an effective radius of 1.5 μm (Clancy et al., 2003; Wolff and Clancy, 2003; Kahre et al., 2006; Madeleine et al., 2011) and an effective variance of 0.3 (Rannou et al., 2006; Madeleine et al., 2011).

Similarly, water ice radiative properties are computed from the refractive indices provided by Warren (1984). In this case, we have selected a log-normal size distribution with an effective radius of 3 μm (Wolff and Clancy, 2003) and effective variance of 0.1 (Wolff and Clancy, 2003; Madeleine et al., 2012). We have assumed a water ice absorption opacity of 0.02 at 12.1 μm, which is a typical value outside the aphelion cloud belt (Smith 2004, Madeleine et al., 2012).

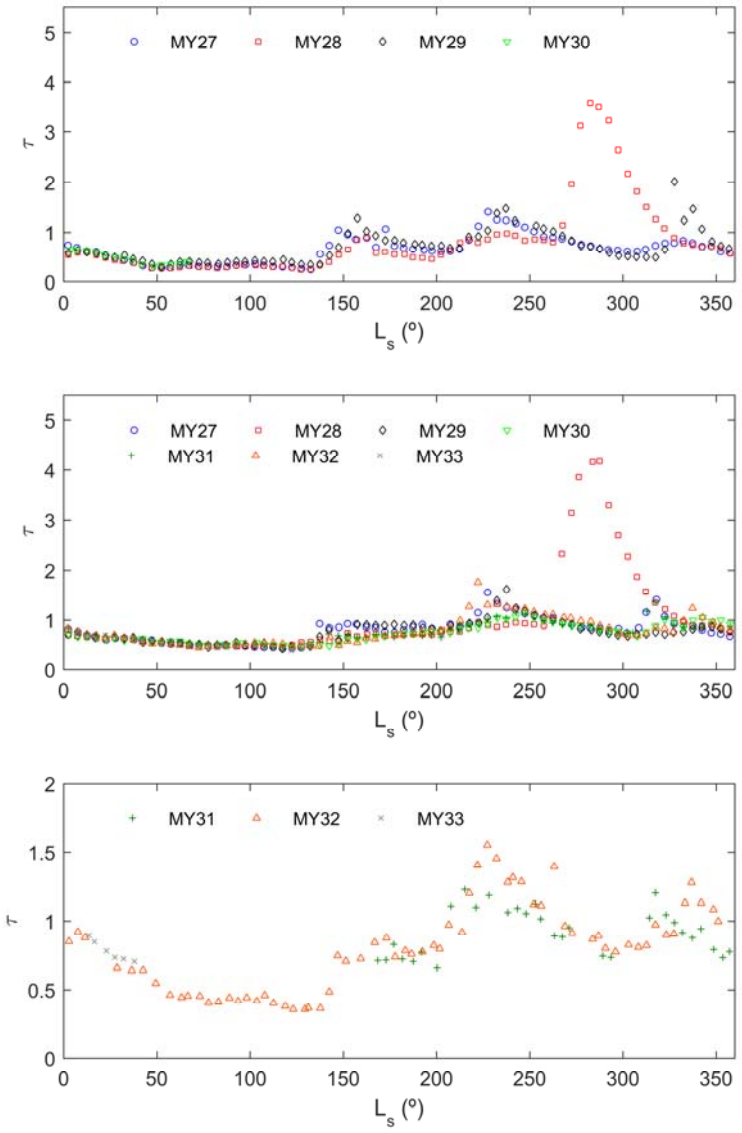

Figure 1. Temporal evolution of the atmospheric opacity at 880 nm at the Spirit (top), Opportunity (middle) and Curiosity (bottom) landing sites, as a function of solar longitude. Note that the vertical axis of the third panel is different from the previous two.

In this article, we have assumed that the retrieved atmospheric opacity at each of the three analyzed landing sites is entirely caused by dust particles. Lemmon et al. (2015) concluded that ice clouds did not show a significant contribution to the atmospheric opacity at the Spirit landing site but that they contributed to the total opacity at the Opportunity site. However, we show that the validity of our assumption is very good to calculate the daily irradiation at the surface.

Table 1. Direct (B), diffuse (D) and total (T) daily irradiations at the Opportunity landing site at L_s = 90º for different relative contributions of water ice clouds to total opacity. Differences with respect to the scenario with only dust are also shown.

% of ice aerosols	Dust opacity	WIC opacity	B (MJ/m^2)	D (MJ/m^2)	T (MJ/m^2)	B/B_0	D/D_0	T/T_0
0	0.440	0.000	6.26	4.47	10.73	1.000	1.000	1.000
10	0.396	0.044	6.25	4.55	10.80	0.998	1.018	1.007
20	0.352	0.088	6.25	4.63	10.88	0.998	1.036	1.014
30	0.308	0.132	6.24	4.72	10.96	0.997	1.056	1.021
40	0.264	0.176	6.23	4.80	11.03	0.995	1.074	1.028
50	0.220	0.220	6.23	4.89	11.12	0.995	1.094	1.036
60	0.176	0.264	6.22	4.97	11.19	0.994	1.112	1.043
100	0.000	0.440	6.19	5.32	11.51	0.989	1.190	1.073

Table 1 shows the direct (B, column 4), diffuse (D, column 5) and total (T, column 6) daily irradiations at a solar longitude L_s = 90º at the Opportunity landing site for a typical clear atmospheric opacity of 0.44 and for different relative contributions of ice aerosols. The last three columns represent the ratio between the direct, diffuse and total daily irradiations for each scenario and their counterparts in the scenario with absence of water ice clouds (denoted as WIC).

These results show that, even for the highest realistic fraction of ice aerosols (60%), differences with the cloud-free scenario are below 1%, 12% and 5% in the direct, diffuse and total irradiations at the surface, respectively. Differences are smaller for the conditions found during most of the year (Smith, 2004). Therefore, we can assume that the retrieved atmospheric opacity is caused by dust particles to calculate the daily irradiation.

3. Temporal and spatial variability of daily irradiation at the top of the atmosphere

In this section we show the daily irradiation at the top of the atmosphere as a function of the time of the year and latitude. The daily irradiation can be calculated using the expression

$$E = \frac{88775}{\pi} E_0 \left[\frac{1 + e\cos\left(L_s - L_{s,p}\right)}{1 - e^2} \right]^2 \left[\left(1 - \sin^2 \varepsilon \sin^2 L_s\right)^{1/2} \cos\phi \sin H + H \sin\varepsilon \sin L_s \sin\phi \right] \quad (1)$$

where E_0 = 590 W/m^2 is the solar irradiance at the mean distance between Mars and the Sun (1.52 AU), e = 0.0934 is the eccentricity of the Martian orbit, ϵ = 25.2º is the obliquity of Mars, $L_{s,p}$ = 251º is the solar longitude at the perihelion, ϕ is the latitude and H is the half of the length of the day expressed in radians calculated as

$$\cos\left(H\right) = -\tan\phi \frac{\sin\varepsilon \sin L_s}{\left(1 - \sin^2 \varepsilon \sin^2 L_s\right)^{1/2}} \quad (2)$$

where if cos (H) is greater than +1 (smaller than -1), then H is 0 (π).

Figure 2 shows the daily irradiation at the top of the atmosphere as a function of latitude and solar longitude. As on Earth, there are polar nights in the winter Hemisphere, annual maximum values are found in polar latitudes in both hemispheres at around their respective summer solstices, and the seasonal variability at low latitudes is lower than at higher latitudes. However, there are some noticeable differences between Mars and our planet. The most striking difference is the stronger asymmetry between the aphelion and the perihelion season on Mars. This is explained by the eccentricity of the Martian orbit, which is higher than on Earth. On a planetary average, the aphelion season is colder than the perihelion season. Moreover, a higher daily insolation causes warmer ground temperatures, which stimulate the lifting of dust from the surface into the atmosphere. Therefore, the most favorable conditions for the formation of dust storms can be found during summer in the Southern Hemisphere. In conclusion, the dichotomy between the relatively cold and clear aphelion season and the relatively warm and dusty perihelion season is mainly caused by the seasonal asymmetries in solar insolation.

It is also interesting to notice that the variability of the insolation at each latitude along the year is clearly higher in the Southern Hemisphere than in the Northern Hemisphere, causing a stronger thermal contrast between summer and winter in the Southern Hemisphere than in the Northern Hemisphere.

4. Results: radiative environment at the MER and MSL landing sites

In this section we show results for the seasonal and interannual daily irradiation at the MERs and MSL landing sites, as well as an analysis of the direct, diffuse and total daily irradiations at the locations of the three rovers. We use atmospheric opacities at 880 nm derived from ground-based measurements of the Pancam instrument onboard the Mars Exploration Rovers (Lemmon et al., 2015) and Mastcam instrument onboard MSL Curiosity rover along with our radiative transfer model to obtain the results mentioned above.

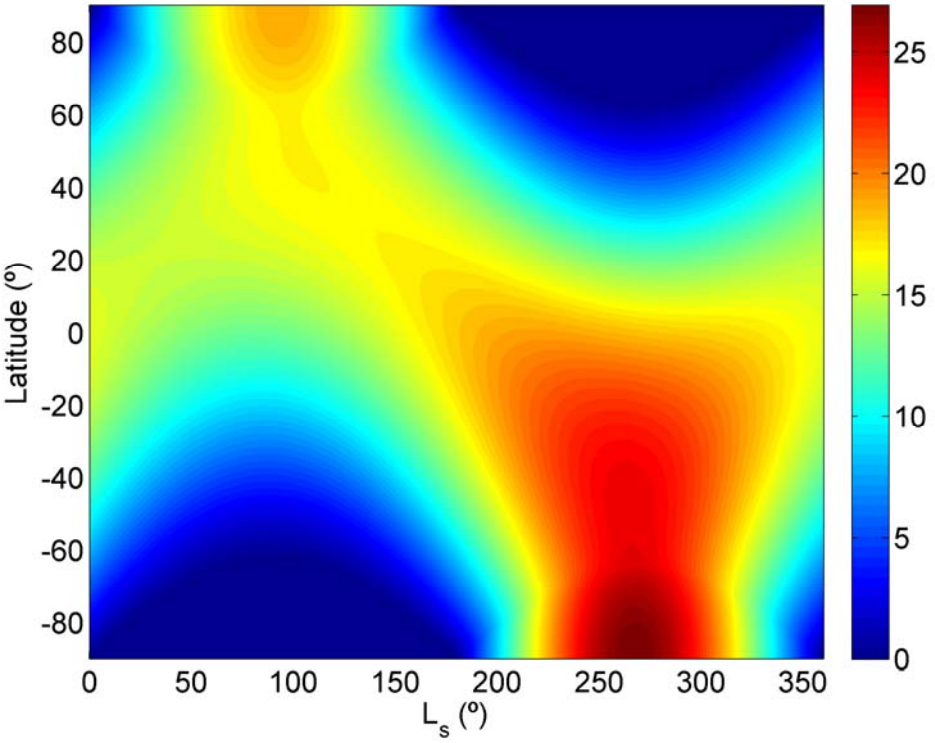

Figure 2. Temporal and spatial variability of daily irradiation (MJ/m^2) at the top of the atmosphere.

We first compare the behavior of total insolation at the Spirit, Opportunity and Curiosity landing sites, and then we analyze further details about the total, direct and diffuse components at each location. Figure 3 shows the daily irradiation at the Spirit (top), Opportunity (middle) and Curiosity (bottom) landing sites. At each site, the lowest annual values occur around the aphelion. At this time, the total insolation is slightly above 8 MJ/m^2 at the Spirit location and above 10 MJ/m^2 at the Opportunity and Curiosity landing sites. On the contrary, the highest daily irradiations occur around the perihelion, with values higher than 17 MJ/m^2 at the Spirit landing site and around 16 MJ/m^2 at the Opportunity and Curiosity locations. Since the radiation at the surface is modulated by the radiation at the top of the atmosphere, the annual amplitude in the daily irradiation is higher at the southernmost location, i.e., at the Spirit landing site. There, the total insolation around the perihelion is more than twice its value around the aphelion; in contrast, at the Opportunity and Curiosity landing sites, the highest annual values are about 60% higher than the lowest annual values.

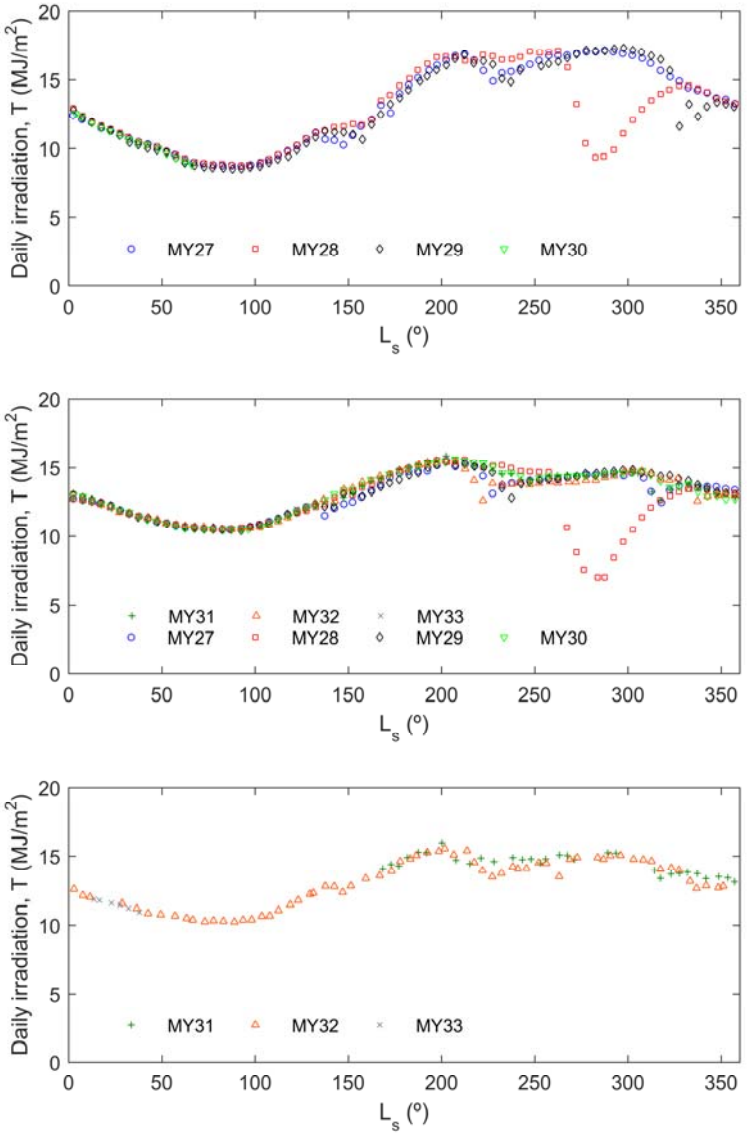

Figure 3. Total daily irradiation at the Spirit (top), Opportunity (middle) and Curiosity (bottom) landing sites.

The most striking feature is the abrupt decrease in the insolation occurred during the second Mars Year of the mission at the Spirit and Opportunity landing sites due to the major dust storm. It is possible to identify other local to regional dust storms that were observed only at one of the MER landing sites, such as the ones that caused a decrease at the Spirit location around $L_s = 155º$ and $L_s = 330º$ during MY 29.

4.1 Spirit landing site

The first panel of Figure 4 shows the ratio between the total irradiation at the surface (T) and the total irradiation at the top of the atmosphere (E) at the Spirit landing site. Except for the perihelion season on MY 28 when a major dust storm occurred, this ratio shows a low seasonal variability, with the surface receiving approximately 80% of the daily irradiation at the top of the atmosphere throughout the year.

The second panel of Figure 4 shows the diffuse daily irradiation (D) at the surface. It presents a strong seasonal variability with annual maximum values occurring during the perihelion season on each year. During the aphelion season, the diffuse irradiation is weaker because the atmosphere is relatively clear (Figure 1, top). The remarkable increase around $L_s = 150º$ is attributed to an increase in atmospheric opacity and to a decrease in the distance between Mars and the Sun. The interannual variability depends on the season, being high close to the perihelion and low close to the aphelion.

The third panel of Figure 4 shows the ratio between the direct irradiation (B) and the diffuse irradiation D. There is a clear dichotomy between the aphelion season, when the atmosphere is relatively clear and the direct component dominates, and the perihelion season, when the atmosphere is dustier and the diffuse component becomes more important than the direct irradiation. The pattern of the aphelion season is repeated every year with small variations.

4.2. Opportunity landing site

The top panel of Figure 5 shows the ratio T/E from MY 27 to MY33. As at the Spirit landing site, approximately 80% of the solar daily irradiation at the top of the atmosphere reaches the surface throughout the year. The small differences between both landing sites are explained by spatial variations in the opacity and by slightly different mean solar zenith angles due to the difference in latitude.

This typical ratio of T/E = 0.8 decreased dramatically during the dust storm occurred during the perihelion season on MY 28 (squares). During this event, the fraction of incoming solar radiation that interacted with the atmospheric aerosols increased markedly, with less than 40% of the total energy at the top of the atmosphere reaching the ground.

The values of the diffuse daily irradiation are shown in the second panel of Figure 5. The seasonal behavior is similar to that at the Spirit landing site, with the lowest annual values occurring in the aphelion season and the highest around the perihelion. However, the annual amplitude is smaller at the Opportunity landing site because it is

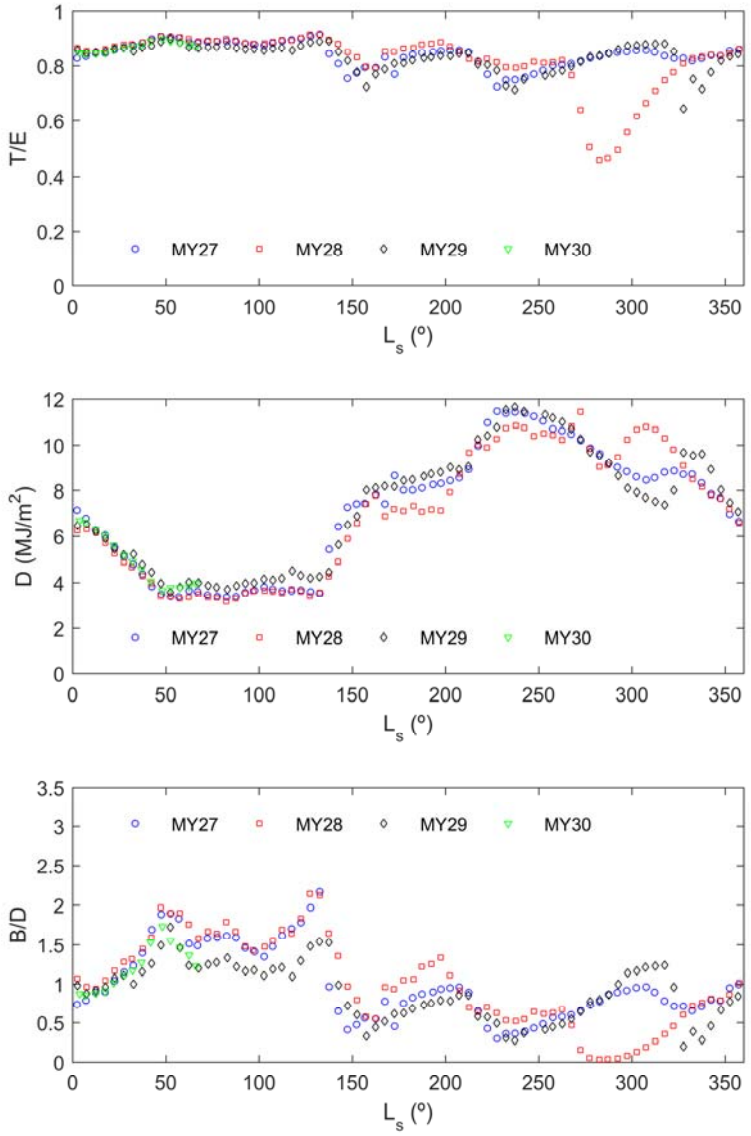

Figure 4. Ratio of total insolation at the surface (T) to that at the top of the atmosphere (E) (upper panel), diffuse daily irradiation D (middle panel), and ratio of direct (B) to diffuse (D) insolation (lower panel) at the Spirit landing site.

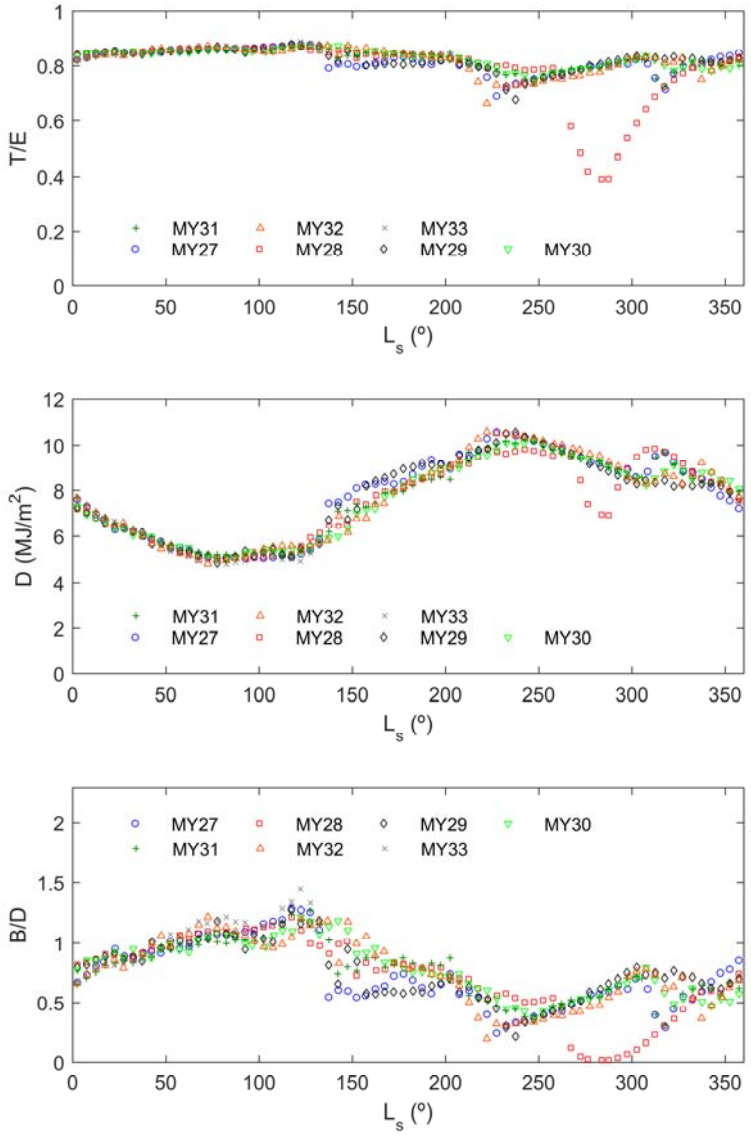

Figure 5. As in Figure 4, but for the Opportunity landing site.

closer to the equator and, therefore, the annual variability at the top of the atmosphere is lower.

Outside major dust storms, the diffuse irradiation at the surface increases with the opacity. However, the opposite behavior is observed during the major dust storm on MY 28, when a local minimum in the amount of diffuse radiation occurred because virtually all the incoming radiation interacted with atmospheric dust, and therefore the fraction of absorbed and reflected radiation by the particles increased significantly.
The ratio B/D is represented in the third panel of Figure 5. Although the qualitative behavior is similar to that at the Spirit location, there is one important difference. At the Opportunity site, this ratio is above one only during a short period of the aphelion season. This is mainly caused by higher opacities at this site (Figure 1, top and middle), which are partly affected by the aphelion cloud belt.

This panel also shows that the interannual variability is very low during the clear season, but that it increases in the perihelion season. It is interesting to notice that during the major dust storm on MY 28, there was virtually no direct radiation reaching the surface at the Mars Exploration Rovers landing sites.

4.3 Curiosity landing site

In the first panel of Figure 6 we show the seasonal evolution of the ratio T/E. This ratio varies between 0.7 during the perihelion season and 0.9 in the clear season. Since the total insolation is also smaller in the aphelion season, we conclude that there is more atmospheric heating due to suspended dust during the perihelion season. This panel also shows that MSL has not been affected by intense dust storms during MY 31 and MY 32.

The seasonal evolution of the diffuse daily irradiation is represented in the second panel of Figure 6. It shows a similar behavior to that at the Opportunity landing site. This was expected, since both latitudes are similar. In fact, the correlation coefficient between the diffuse daily irradiations at both landing sites is $R^2 = 0.94$.

The third panel of Figure 6 shows the variability of the ratio B/D. During the perihelion season, the diffuse component is always larger than the direct component, and a low interannual variability is observed. At the MSL landing site, in contrast to Opportunity, the direct irradiation is higher than the diffuse one during a large fraction of the aphelion season. This is a consequence of a smaller atmospheric opacity, which could be partially explained by a smaller influence of water ice clouds.

5. Conclusions

In this article we have used our radiative transfer model COMIMART and in-situ measurements of atmospheric opacity to characterize the radiative environment at the landing sites of the Mars Exploration Rovers (Spirit and Opportunity) and Mars Science Laboratory (Curiosity) missions.

The interannual variability of the daily irradiation at the surface of each of the three landing sites is relatively low. The exception occurred on MY 28, when a major dust storm evolved. At seasonal time scales, the variability of the daily irradiation is

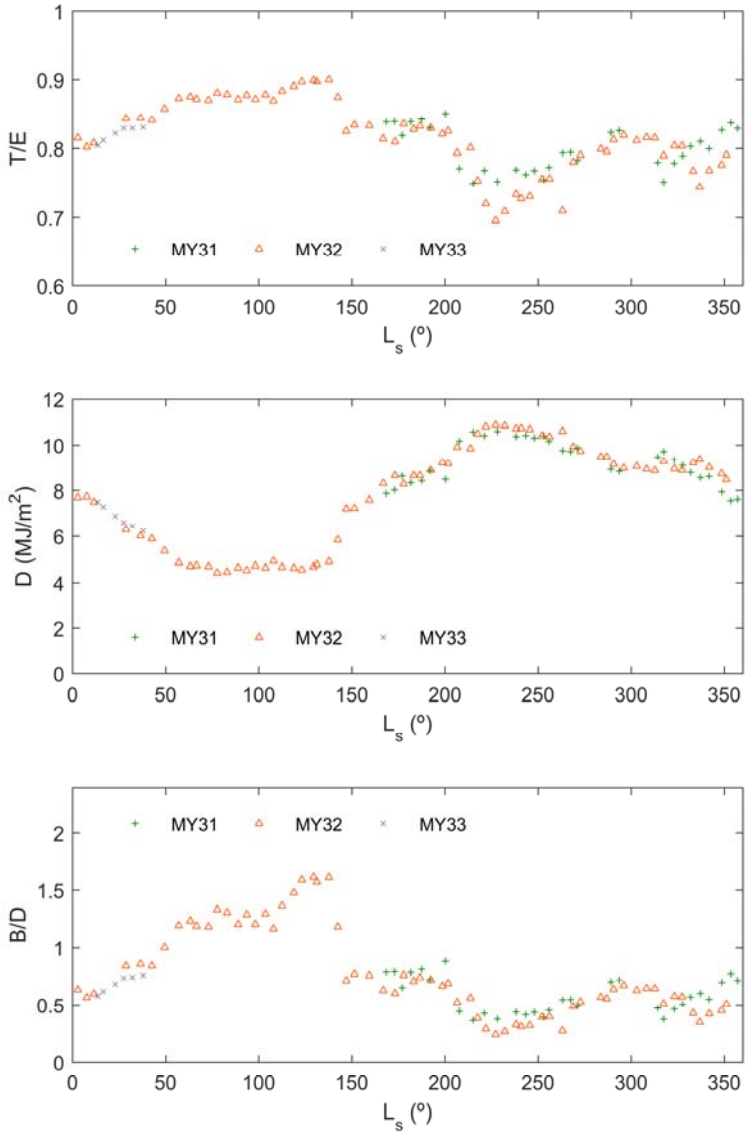

Figure 6. As in Figure 4, but for the Curiosity landing site. The reader is referred to Martínez et al. (2016; this issue) for an analysis of the ultraviolet insolation at the MSL landing site.

higher during the perihelion season, when the amount of suspended dust is usually relatively high. In contrast, the radiative environment during the aphelion season shows a very similar behavior every Martian year.

A dichotomy in the relative importance of the direct and diffuse components is observed at the three landing sites. During the aphelion season, the atmosphere is relatively clear and direct radiation prevails. In contrast, the higher amount of dust in the atmosphere during the perihelion season leads to a higher fraction of the incoming radiation being scattered, and hence the direct radiation diminishes, becoming the diffuse component more important.

Characterization of the seasonal and interannual variability of the daily irradiation at the surface is very important to prepare for future human exploration of Mars. It allows quantifying the daily doses of ultraviolet radiation and their potential effects on astronauts, which is necessary prior sending manned missions to Mars, and it also contributes to understand the thermodynamic processes of the atmosphere as well as, in longer time scales, the climate of Mars. To these ends, the solar radiation at the surface will be measured in several bands of the shortwave spectrum by the ExoMars 2020 (http://exploration.esa.int/jump.cfm?oid=56933) and Mars 2020 (Apéstigue et al. 2015) missions, complementing and expanding the solar radiation dataset derived from MER and MSL measurements.

Acknowledgements

This work has been partially supported by the research projects AYA2011-29967-C05-02 and CGL2011-25327. The author A. Vicente-Retortillo wishes to acknowledge the Spanish Ministry of Economy and Competitiveness (MINECO) for the granted FPI fellowship (BES-2012-059241).

References

APÉSTIGUE, V., ARRUEGO, I., MARTÍNEZ, J., JIMÉNEZ, J. J., RIVAS, J. et al. (2015). Radiation and Dust Sensor for MARS2020: technical design and development status overview. European Planetary Science Congress 2015, 27 September - 2 October, 2015, Nantes, France. Vol. 10, EPSC2015-813.

CLANCY, R.T., WOLFF, M. J., CHRISTENSEN, P. R. (2003). Mars aerosol studies with the MGS TES emission phase function observations: optical depths, particle sizes, and ice cloud types versus latitude and solar longitude. *J. Geophys. Res.*, 108, 5098, doi: 10.1029/2003JE002058.

COLBURN, D. S., POLLACK, J. B., HABERLE, R. M. (1989). Diurnal variations in optical depth at Mars. *Icarus*, 79 (1), 159-189, doi: 10.1016/0019-1035(89)90114-0.

CÓRDOBA-JABONERO, C., LARA, L. M., MANCHO, A. M., MÁRQUEZ, A., RODRIGO, R. (2003). Solar ultraviolet transfer in the Martian atmosphere: biological and geological implications. *Planet. Space Sci*., 51 (6), 399–410, doi: 10.1016/S0032-0633(03)00023-0.

HANEL, R., CONRATH, B., HOVIS, W., KUNDE, V., LOWMAN, P. et al. (1972). Investigation of the Martian environment by infrared spectroscopy on Mariner 9. *Icarus,* 17, 423–42, doi: 10.1016/0019-1035(72)90009-7.

HANSEN, J.E., TRAVIS, L. D. (1974). Light scattering in planetary atmospheres. *Space Sci. Rev*., 16, 527–610.

KAHRE, M. A., MURPHY, J. R., HABERLE, R. M. (2006). Modeling the Martian dust cycle and surface dust reservoirs with the NASA Ames general circulation model. *J. Geophys. Res*.,111, E06008, doi: 10.1029/2005JE002588.

LEMMON, M. T., WOLFF, M. J., BELL III, J. F., SMITH, M. D., CANTOR, B. A., SMITH, P. H. (2015). Dust aerosol, clouds, and the atmospheric optical depth record over 5 Mars years of the Mars Exploration Rover mission. *Icarus*, 251, 96–111, doi: 10.1016/j.icarus.2014.03.029.

MADELEINE, J.-B., FORGET, F., MILLOUR, E., MONTABONE, L., WOLFF, M. J. (2011). Revisiting the radiative impact of dust on Mars using the LMD Global Climate Model. *J. Geophys. Res*., 116, E11010, doi: 10.1029/2011JE003855.

MADELEINE, J.-B., FORGET, F., MILLOUR, E., NAVARRO, T., SPIGA, A. (2012). The influence of radiatively active water ice clouds on the Martian climate. *Geophys. Res. Lett*., 39, L23202, doi: 10.1029/2012GL053564.

MARTIN, T. Z., RICHARDSON, M. I. (1993). New dust opacity mapping from Viking infrared thermal mapper data. *J. Geophys. Res.* 98:10941–49, doi: 10.1029/93JE01044.

MARTÍNEZ, G. M., VALERO, F., VÁZQUEZ, L. (2009). Characterization of the Martian surface layer. *J. Atmos. Sci*., 66 (1), 187–198, doi: 10.1175/2008JAS2765.1.

MARTÍNEZ, G. M., VALERO, F., L. VÁZQUEZ, L. (2011). The TKE budget in the convective Martian planetary boundary layer. *Q. J. R. Meteorol. Soc*., 137 (661), 2194–2208, doi: 10.1002/qj.883.

MARTÍNEZ, G. M., RENNÓ, N., FISCHER, E., BORLINA, C. S., HALLET, B. et al. (2014). Surface energy budget and thermal inertia at Gale Crater: calculations from ground-based measurements. *J. Geophys. Res. [Planets]*, 119 (8), 1822–1838, doi: 10.1002/2014JE004618.

MARTÍNEZ, G. M., DE LA TORRE, M., VICENTE-RETORTILLO, A., KEMPPINEN, O., RENNO, N., LEMMON, M. (2016). An overview of the environmental conditions at Gale Crater from MSL/REMS measurements. *Física de la Tierra*, this issue.

MONTABONE, L., FORGET, F., MILLOUR, E., WILSON, R. J., LEWIS, S. R. et al. (2015). Eight-year climatology of dust optical depth on Mars. *Icarus*, 251, 65-95, doi: 10.1016/j.icarus.2014.12.034.

PETROSYAN, A., GALPERIN, B., LARSEN, S. E., LEWIS, S. R., MÄÄTTÄNEN, A. et al. (2011). The Martian atmospheric boundary layer. *Rev. Geophys.,* 49 (3), RG3005, doi: 10.1029/2010RG000351.

RANNOU, P., PERRIER, S., BERTAUX, J. L., MONTMESSIN, F., KORABLEV, O., RÉBÉRAC, A. (2006). Dust and cloud detection at the Mars limb with UV scattered sunlight with SPICAM. *J. Geophys. Res.*, 111, E09S10, doi: 10.1029/2006JE002693.

READ, P. L., LEWIS, S. R. (2004). The Martian climate revisited: atmosphere and environment of a desert planet, Springer-Verlag, Berlin, ISBN: 978-3-540-40743-0.

SAVIJÄRVI, H., KAUHANEN, J. (2008). Surface and boundary layer modelling for the Mars Exploration Rover sites. *Q. J. R. Meteorol. Soc.*, 134 (632), 635–641, doi: 10.1002/qj.232.

SMITH, M. D. (2004). Interannual variability in TES atmospheric observations of Mars during 1999–2003. *Icarus*, 167 (1), 148–165, doi: 10.1016/j.icarus.2003.09.010.

SMITH, M. D. (2009). THEMIS observations of Mars aerosol optical depth from 2002–2008. *Icarus*, 202(2), 444-452, doi: 10.1016/j.icarus.2009.03.027.

SMITH, P. H., LEMMON, M. T. (1999). Opacity of the Martian atmosphere measured by the imager for Mars Pathfinder. *J. Geophys. Res.* 104, 8975–8985, doi: 10.1029/1998JE900017.

VICENTE-RETORTILLO, Á., VALERO, F., VÁZQUEZ, L., MARTÍNEZ, G. M. (2015). A model to calculate solar radiation fluxes on the Martian surface. *J. Space Weather Space Clim.*, 5, A33, doi: 10.1051/swsc/2015035.

WARREN, S. G. (1984). Optical constants of ice from the ultraviolet to the microwave. *Appl. Opt*., 23 (8), 1206–1225, doi: 10.1364/AO.23.001206.

WOLFF, M. J., CLANCY, R. T. (2003). Constraints on the size of Martian aerosols from Thermal Emission Spectrometer observations. *J. Geophys. Res.*, 108, 5097, doi: 10.1029/2003JE002057.

WOLFF, M. J., SMITH, M. D., CLANCY, R. T., ARVIDSON, R., KAHRE, M., SEELOS IV, F., MURCHIE, S., SAVIJÄRVI, H. (2009). Wavelength dependence of dust aerosol single scattering albedo as observed by the Compact Reconnaissance Imaging Spectrometer. *J. Geophys. Res.*, 114, E00D04, doi: 10.1029/2009JE003350.

WOLFF, M. J., CLANCY, R. T., GOGUEN, J. D., MALIN, M. C., CANTOR, B. A. (2010). Ultraviolet dust aerosol properties as observed by MARCI. *Icarus*, 208 (1), 143–155, doi: 10.1016/j.icarus.2010.01.010.